J Opt (September 2023) 52(3):1197–1205
https://doi.org/10.1007/s12596-022-00937-6

RESEARCH ARTICLE

SPR-based PCF sensor with embedded silver wires for wide range temperature sensing

Lin Yang[1] · Chunjie Hu[2] · YuYang Zhao[3] · Zao Yi[4] · Qiang Liu[1] · Chao Liu[1] · Jingwei Lv[1] · Paul K. Chu[5]

Received: 27 May 2022 / Accepted: 23 July 2022 / Published online: 3 September 2022

Abstract A photonic crystal fiber (PCF) temperature sensor consisting of dual embedded silver wires and based on surface plasmon resonance is designed and investigated by the finite element method. The ionic liquid [BMim] [PF6] and Ag are chosen as the filling liquid and sensitive material, respectively. The properties of the sensors based on the single PCF structure and dual symmetrical PCF structure are determined and discussed. The single PCF structure shows an average spectral sensitivity of 2.033 nm/°C, maximum sensitivity of 3.900 nm/°C, and temperature resolution of 0.0256 °C, whereas the dual symmetrical PCF device has an average spectral sensitivity of 3.166 nm/°C, maximum sensitivity of 5.000 nm/°C, and temperature resolution of 0.0200 °C. In addition, the proposed sensor can realize a extremely wide temperature sensing range of 20–320 °C.

Keywords PCF-SPR · Ionic liquid [BMim] [PF6] · Temperature · Finite element method (FEM)

✉ Chao Liu
msm-liu@126.com

1 School of Physics and Electronic Engineering, Northeast Petroleum University, Daqing 163318, People's Republic of China

2 Department of Gynecology and Obstetrics, The Fourth Affiliated Hospital of Harbin Medical University, Harbin 150001, People's Republic of China

3 Department of Space Information Division of China Transportation Telecommunication Information, Beijing 100000, People's Republic of China

4 Joint Laboratory for Extreme Conditions Matter Properties, Southwest University of Science and Technology, Mianyang 621010, People's Republic of China

5 Department of Physics, Department of Materials Science and Engineering, and Department of Biomedical Engineering, City University of Hong Kong, Tat Chee Avenue, Kowloon, Hong Kong, People's Republic of China

Introduction

Surface plasmon resonance (SPR) arises from free electron oscillations between metallic and dielectric materials excited by the incident TM wave or P-polarized light. The SPR technology is widely applied to biology, chemistry, medicine, and environment science due to advantages such as the high refractive index sensitivity and resolution, real-time monitoring, and non-label detection [1–5]. The prism-based sensor based on surface plasmon resonance was first proposed by Krestchmann in 1968 [6, 7] but this conventional configuration is quite bulky and difficult to miniaturize. Recently, optical fiber sensors with the possibility of miniaturization make portable sensing and continuous monitoring possible. Compared with the traditional single-mode fiber, the photonic crystal fiber (PCF) has many distinctive features including the large mode area and high birefringence [8–12]. The air holes in the direction of light propagation can more easily provide the phase matching conditions between the core-guided mode and SPP mode. In this way, the energy of the fiber core can be coupled with the plasma [13–15] on the metal surface and the loss spectrum can be used for detection [16]. The PCF sensors based on surface plasmon resonance have many potential applications such as refractive index and temperature sensors [17–19], absorbers [20], waveguides [21, 22], photonic quasi-crystal fiber (PQF) sensors [23–26], and other devices. Several PCF-SPR temperature sensors have been proposed. For instance, Zhao et al. [27] reported a fiber-optics SPR sensor filled with anhydrous ethanol and a thin silver film was coated on the unclad part of the MMF to achieve a sensitivity of 1.5745 nm/°C. Luan et al. [28]

designed a six-hole PCF-SPR sensor with silver nanowires and the PCF holes were filled with the mixture liquid of ethanol and chloroform to yield a large thermo-optical coefficient and high temperature sensitivity of 4 nm/K. Siddik A B et al. [29] proposed a dual-core PCF temperature sensor, the major objective of this design is to increase the average sensitivity and it can achieve a high sensitive of 2.25 nm/°C. MR Islam et al. [30] offer an external sensing approach of PCF-SPR sensor with a thin layer of TiO_2 laminated in the midst of the fiber and the gold layer. The sensors mentioned above exhibit good sensing characteristics and contribute to the progress of PCF SPR temperature sensor. However, the maximum temperature sensing range of the above sensors is only about 60 °C. More sensors have to be produced to meet the detection of different temperature ranges. Although advances pertaining to the manufacturing and post-processing technology of optical fibers have spurred substantial development in techniques, it is not easy to fabricate a large variety of PCF sensors. Therefore, the design of a large-range temperature detection sensor which can satisfy the demand for multiple temperature sensing is quite necessary.

In this work, a PCF-SPR temperature sensor comprising dual embedded silver wires is designed with the ionic liquid 1-butyl-3-methylimidazolium hexafluorophosphate [BMim] [PF6] as the filling liquid in order to achieve an extremely wide sensing range of 20–320 °C. This structure overcomes the poor sensing performance stemming from uneven metal coatings. To optimize the temperature sensing properties, numerical simulation is performed on the single PCF structure and dual symmetrical PCF structure. Compared to the single PCF structure, the energy transfer to silver wires in the dual symmetrical PCF device is enhanced and the latter thus has better properties such as an average spectral sensitivity of 3.166 nm/°C, maximum sensitivity of 5.000 nm/°C and temperature resolution of 0.0200 °C.

Numerical model and simulation

Numerical analysis is carried out using the COMSOL Multiphysics software by the finite element method (FEM). Figure 1 shows the cross section of the PCF-SPR temperature sensor with dual embedded silver wires. There are 24 regular air holes in the cladding of the fiber and the radii of the PCF and air holes are $R = 5.5$ μm and $r_1 = 0.3$ μm, respectively. The distance of adjacent air holes is $s = 1$ μm. Silver is chosen as the surface plasmon materials because of the excellent chemical properties. Double symmetrical corroded channels are placed in the dual identical silver wires following corrosion with hydrofluoric acid. The permittivity of the silver is calculated by the Drude-Lorentz model [31]:

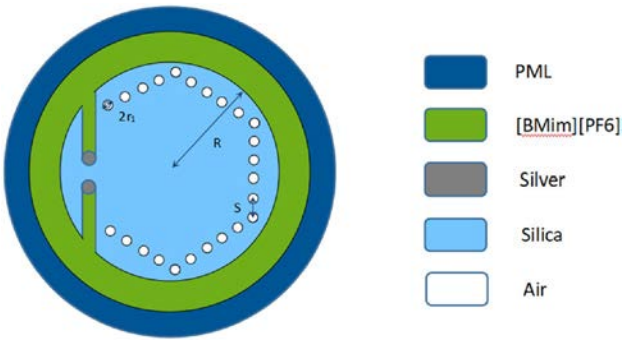

Fig. 1 Cross section of the PCF-SPR temperature sensor with dual embedded silver wires

$$\varepsilon_{\mathrm{Ag}} = \varepsilon_1 - \frac{\omega_p^2}{\omega\left(\omega + i\gamma_D\right)} - \sum_{m=1}^{5} \frac{f_m \cdot \omega_m^2}{\omega_m^2 - \omega^2 - i\gamma_m\omega} \tag{1}$$

where $\varepsilon_1 = 2.1485$, $\omega_p = 9.1821$ eV, $\gamma_p = 0.0210$ eV, ω_1, ω_2, ω_3, ω_4, and ω_5 are 4.180 eV, 4.5309 eV, 5.0094 eV, 5.7530 eV, and 6.9104 eV, respectively, f_1, f_2, f_3, f_4, and f_5 are 0.1227, 0.2167, 0.2925, 0.4305, and 0.6943, respectively, $\gamma_1 = 0.2659$ eV, $\gamma_2 = 0.4269$ eV, $\gamma_3 = 0.6929$ eV, $\gamma_4 = 1.1210$ eV, and $\gamma_5 = 1.3410$ eV.

Silica is the basic materials of the PCF and the dispersion relation of silica is determined by Sellmeier equation [31]:

$$n^2 = 1 + \frac{A_1\lambda^2}{\lambda^2 - B_1^2} + \frac{A_2\lambda^2}{\lambda^2 - B_2^2} + \frac{A_3\lambda^2}{\lambda^2 - B_3^2} \tag{2}$$

where λ stands for the vacuum wavelength of the incident light in micrometer (μm), $A_1 = 0.696166300$, $A_2 = 0.407942600$, $A_3 = 0.897479400$, $B_1 = 4.67914826 \times 10^{-3}\mu m^2$, $B_2 = 1.35120631 \times 10^{-2}\mu m^2$, and $B_3 = 97.9340025\ \mu m^2$. The ionic liquid [BMim] [PF6] is chosen as the temperature sensitive liquid because of the low vapor pressure, low volatility, low melting point, wide operating range [6–340 °C], as well as good thermal stability. The temperature sensitivity coefficient of the ionic liquid [BMim] [PF6] can reach -2.635×10^{-4} [32] and the relationship between the refractive index ($n_{[\mathrm{BMim}]\,[\mathrm{PF6}]}$) and temperature is shown in the following[32–34]:

$$n_{[\mathrm{BMim}]\,[\mathrm{PF_6}]} = 1.41025 - 0.0002635(T - 20) \tag{3}$$

where T presents the temperature range from 20 to 320 °C. In the simulation, a perfectly matched layer (PML) is adopted as the artificial boundary condition to absorb scattered light. The confinement loss of the PCF is calculated by the refractive index matching method using the following Eq. [35]:

$$\alpha_{\mathrm{loss}} = 8.686 \times \frac{2\pi}{\lambda}\mathrm{Im}[n_{\mathrm{eff}}] \times 10^4(\mathrm{dB/cm}) \tag{4}$$

where λ is the wavelength of the vacuum incident light on the micrometer scale and $Im(n_{eff})$ is the imaginary part of the effective refractive index of the core-guide mode.

Results and discussion

The size of the air holes is one of important parameters of sensors as it affects the variation in the resonant wavelength and confinement loss spectra when the temperature changes. Figure 2 shows the confinement loss spectra when the radius of the air holes r_1 changes from 0.1 to 0.4 μm in the temperature range between 20 and 320 °C. The resonant wavelength red-shifts and the changes in the resonant peak between 20 and 320 °C are 0.31 μm, 0.52 μm, 0.61 μm, 0.62 μm when the radius of the air holes goes up from 0.1 to 0.4 μm. It is because the contact surface between the air holes and filling ionic liquid [BMim] [PF6] increases when the air holes are larger. The variation in the resonant peak shows a bigger difference from 20 to 320 °C, but the difference in the wavelength variation between $r_1 = 0.3$ μm and $r_1 = 0.4$ μm is much smaller than those in other cases. The variation in the resonant wavelength between 20 and 320 °C

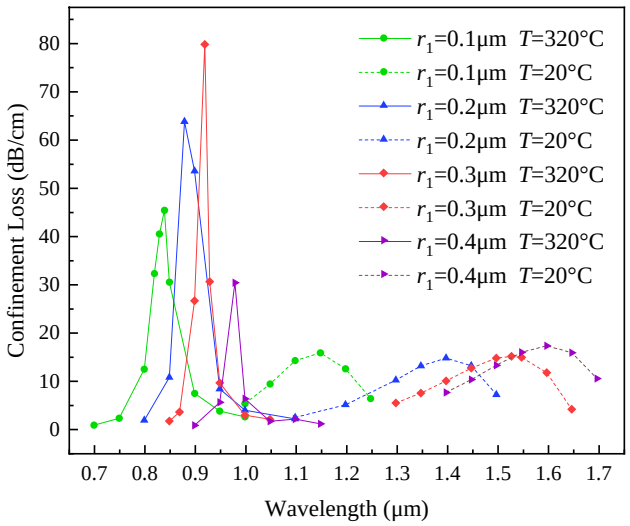

Fig. 2 Confinement loss spectra of the sensors with different air holes from 20 to 320 °C

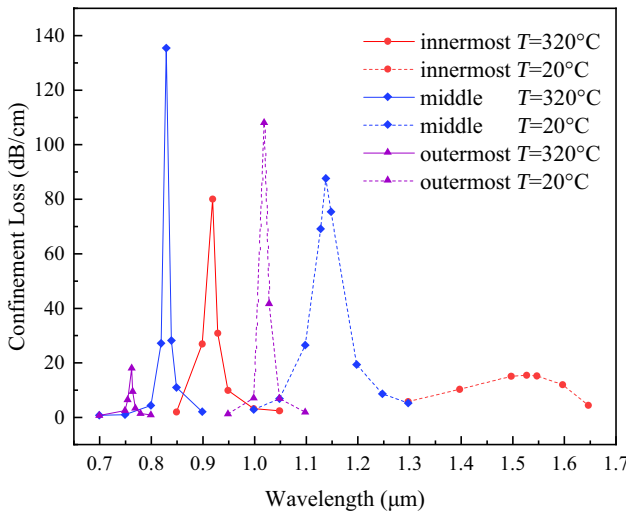

Fig. 3 Confinement loss spectra of the sensor for different corroded depths from 20 to 320 °C

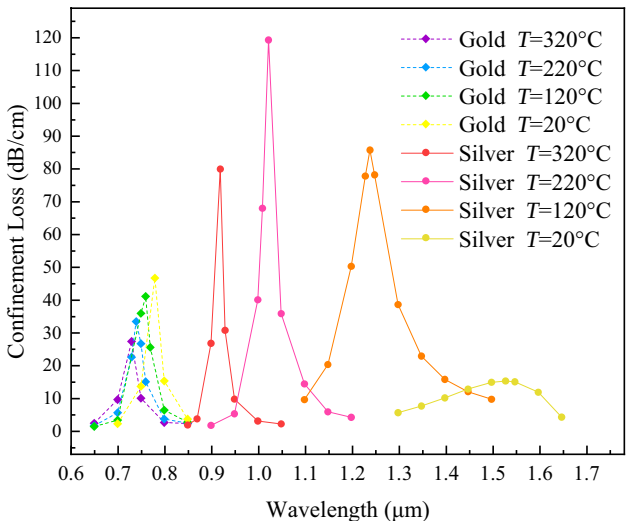

Fig. 4 Confinement loss spectra of the sensor for different metal materials (gold and silver) from 20 to 320 °C

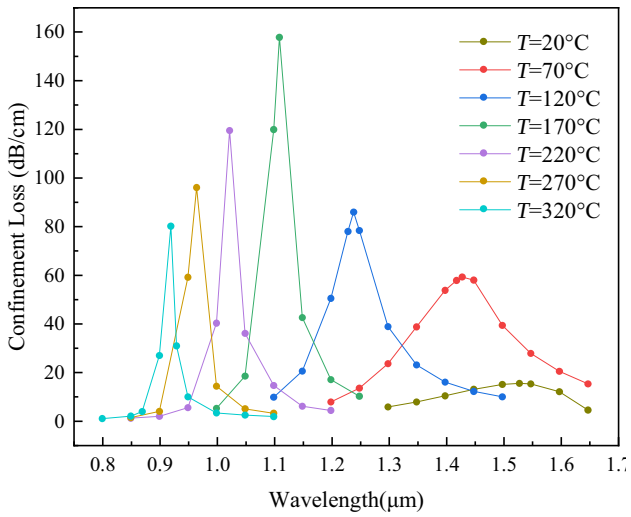

Fig. 5 Confinement loss spectra of the sensor when the temperature changes from 20 to 320 °C

is almost the maximum when r_1 is 0.3 μm and the optimal air hole radius is 0.3 μm.

Surface plasmon resonance is excited at the double symmetrical corroded channels where metal (silver) wires are placed and the influence of the depths of the corroded channels is shown as Fig. 3. Resonance moves towards longer wavelengths with increasing corroded depths because the distance of dual silver wires narrows for a larger corroded depth and stronger coupling occurs. Besides, with increasing corroded depths, energy is transferred more easily

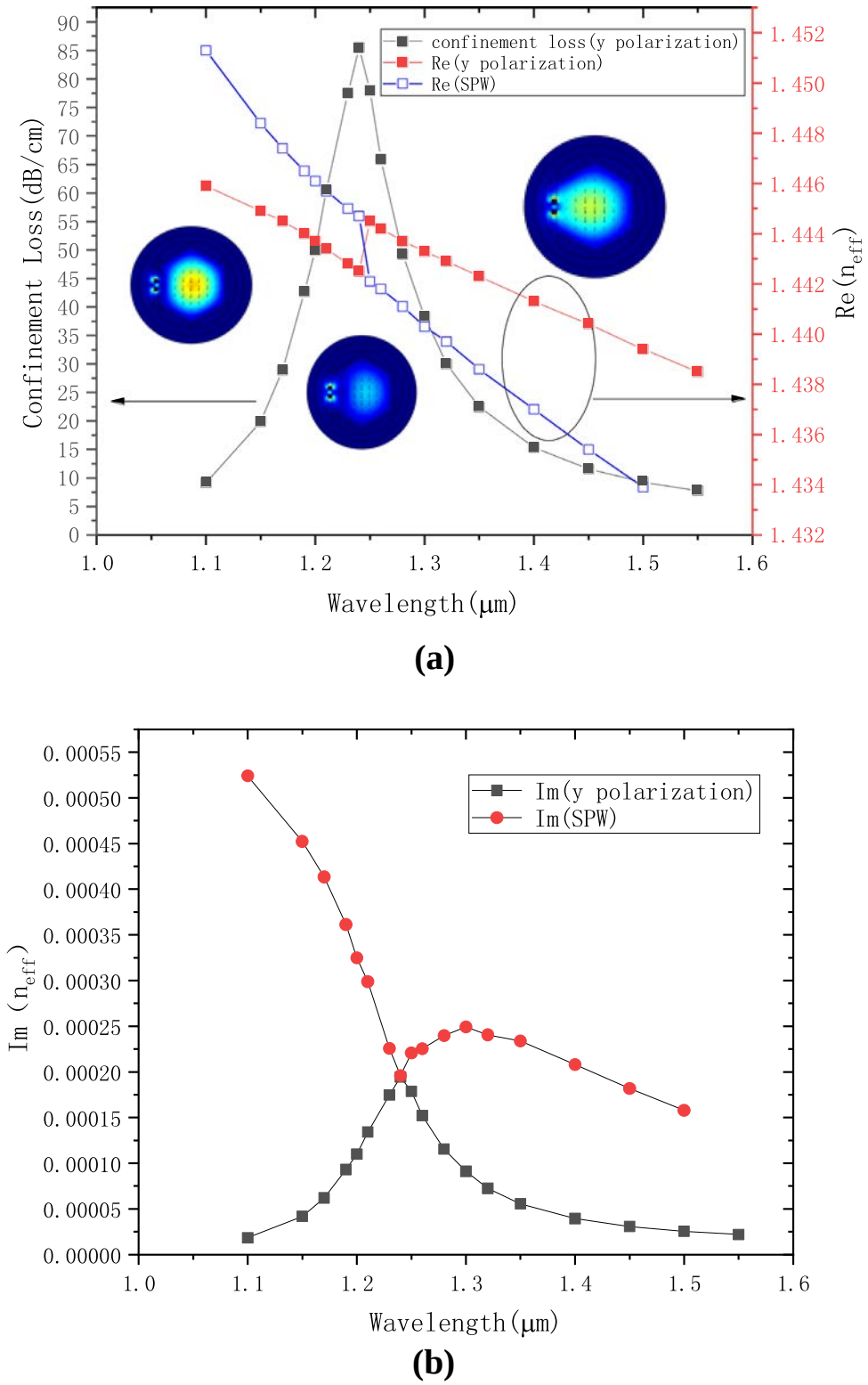

Fig. 6 **a** Confinement loss spectra of fundamental mode when the temperature is 120 °C **b** Imaginary part of the effective refractive index of the fundamental mode

from the core-guide mode to the SPP mode and the variation in the resonant wavelength between 20 and 320 °C can reach 0.61 μm for the largest depth. The performance of different metal materials is shown in Fig. 4. Gold and silver are usually selected as the plasmonic materials to excite SPR and the permittivity of gold in the near-infrared region is given by the Drude model [36]. It is obvious that silver wires are better than gold wires as there are only tiny variations in the resonant wavelength with gold wires. The sensor is thus composed of silver wires and the filling ionic liquid [BMim] [PF6] generated by corrosion and oxidation.

Figure 5 presents the confinement loss spectra of the sensor with the single PCF structure for the temperature range from 20 to 320 °C. A blue-shift is observed from the resonant wavelength because the refractive index of the filling ionic liquid [BMim] [PF6] decreases with increasing temperature. The loss peak increases initially from 20 to 170 °C and then decreases from 170 to 320 °C. Complete coupling between the core-guided mode and SPP mode can be achieved at 170 °C to yield the maximum loss peak of 157.67 dB/cm. In addition, the average and maximum spectral sensitivities can reach 2.033 nm/°C and 3.900 nm/°C, respectively, and the corresponding temperature resolution is 0.0256 °C. The spectral sensitivity is expressed by the following equation [37]:

$$S_\lambda = \frac{\Delta\lambda_{\text{peak}}}{\Delta T}(\text{nm}/^\circ\text{C}) \tag{5}$$

where $\Delta\lambda_{\text{peak}}$ is the change of the resonant wavelength and ΔT is the temperature variation. The temperature resolution (R) is defined as [37]:

$$R = \frac{\Delta T \Delta\lambda_{\text{min}}}{\Delta\lambda_{\text{peak}}}(^\circ\text{C}) \tag{6}$$

where $\Delta\lambda_{\text{min}}$ is the minimum spectral resolution assumed to be 0.1 nm, $\Delta\lambda_{\text{peak}}$ stands for the change of resonant wavelength, and ΔT represents the temperature difference.

Figure 6(a) shows the confinement loss spectra of fundamental mode in y-direction at a temperature of 120 °C. It can be seen that the silver nanowires, which generate surface plasmon resonance are located on the side of the fiber. Therefore, the resonance caused by the fundamental mode of y polarization is stronger. In Fig. 6(b), we can see that the imaginary part of the effective refractive index of the fundamental mode and the SPW mode have an intersection at the wavelength of 1245 nm. The energy fully coupled state is achieved at the anti-intersection point of the phase matching condition.

The characteristic of sensor with only one silver wire is also studied. As shown in Fig. 7, while there is a silver wire on only one side, the polarization direction of the fundamental mode changes with the increasing wavelengths.

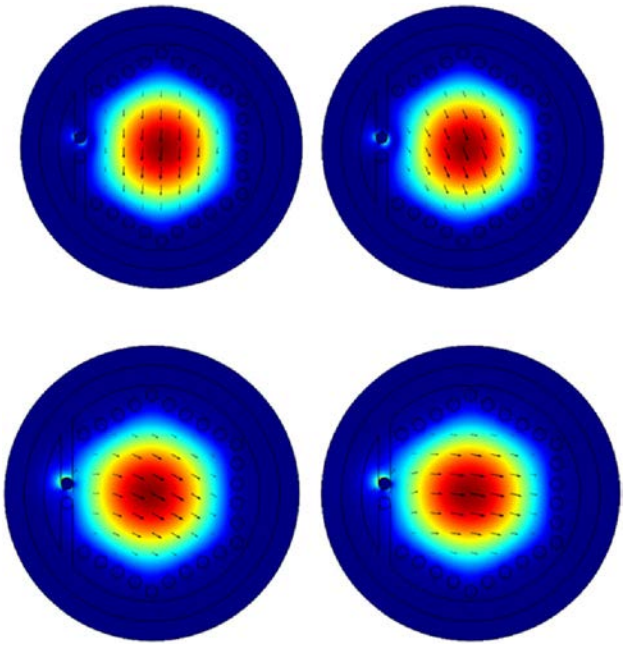

Fig. 7 The polarization direction of the fundamental mode with only one silver wire

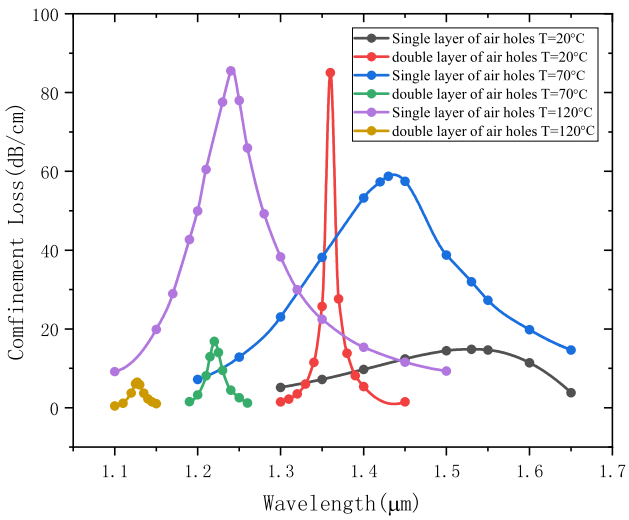

Fig. 8 The confinement loss of the sensor with two layers of air holes

The polarization direction will gradually be deflected in a counterclockwise direction with the increasing wavelength of the incident light, and there will be a phenomenon of false mode. Theoretically, the two electric fields polarization directions of fundamental mode should be orthogonal to each other. However, while there is a single-sided silver wire, the loss of one polarization is extremely large, the other polarization mode will have a tendency to parallelize, and the angle of the polarization directions becomes an acute angle. The polarization directions of non-orthogonality

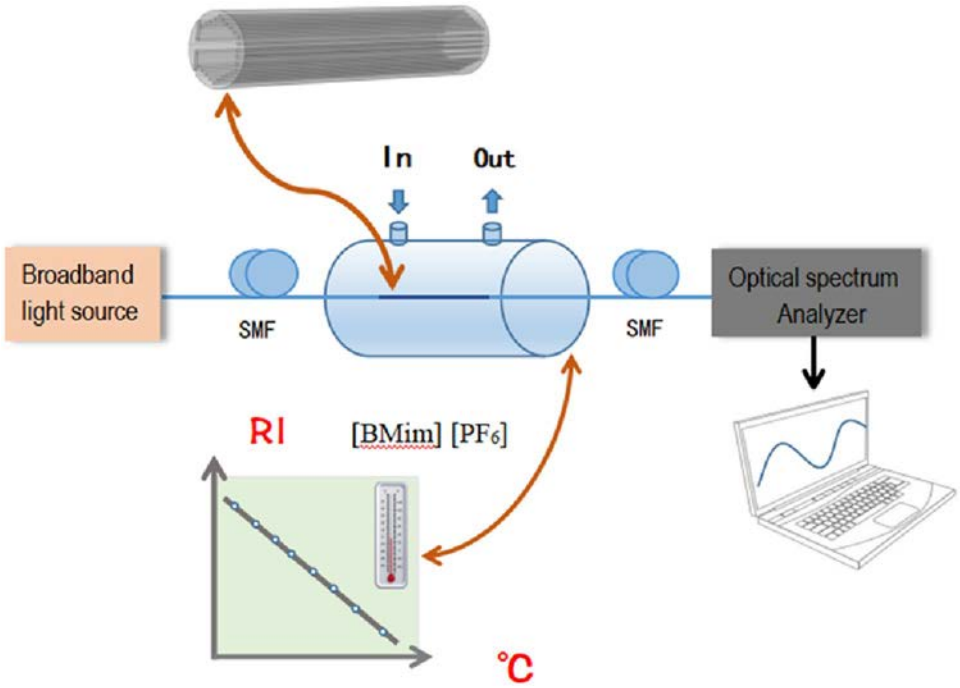

Fig. 9 Schematic diagram of the proposed experimental setup

indicating that single-sided silver wire should not be used as a sensing structure.

Figure 8 shows the confinement loss of the sensor with two layers of air holes. The radius of the air holes is 0.3 μm, and the spacing is 1 μm. The y-polarized fundamental mode shows a blue shift and the loss energy rapidly decreases with the increasing temperature. While the temperature is above 120 °C, the energy loss can be ignored for that the refractive index of the temperature-sensitive liquid decreases at a high temperature. We can also see that the maximum light energy is confined to the fiber core at low temperatures, and the peak width at half-height becomes narrower. In addition, the inner air holes reduce the area of the sensor core, which further increases the requirements for the penetration distance of the evanescent wave.

Figure 9 shows the schematic diagram of proposed sensor set-up. The experimental measurement is mainly composed of four parts. Broadband light source (BBS) and single-mode fiber (SMF) are used as light source emitting device

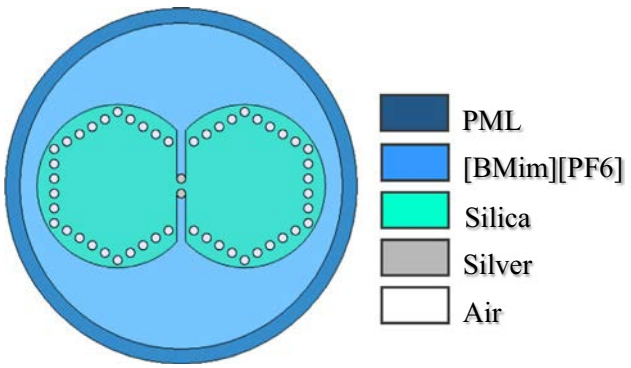

Fig. 10 Cross section of the symmetrical PCF SPR temperature sensor with dual embedded silver wires

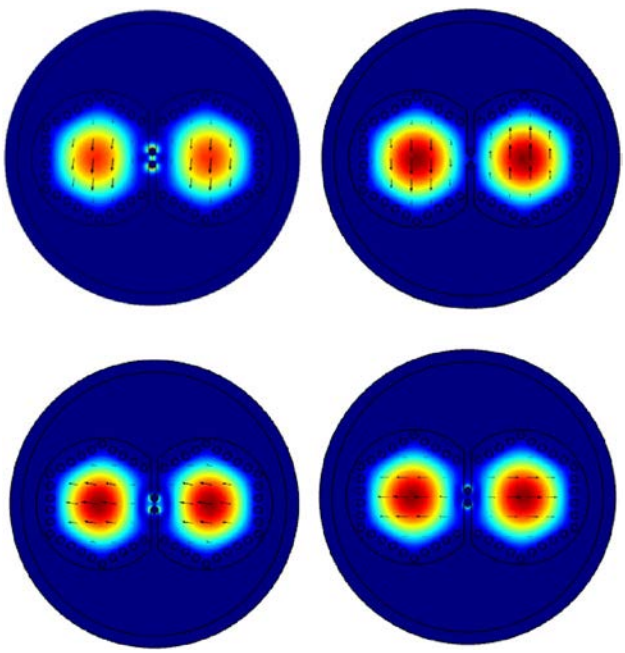

Fig. 11 Electric field distribution of four modes of dual symmetrical PCF

Fig. 13 Fitted polynomial curves for the resonant wavelength and temperature: **a** Comparison of the two structure; **b** Single PCF structure; **c** Dual symmetrical PCF structure

and transmission optical path, respectively. The ionic liquid [BMim] [PF6] is selected as temperature sensitive material and its refractive index is negatively correlated with ambient temperature. The proposed sensor is placed in the liquid, and the temperature is monitored by detecting the refractive index of the liquid. Optical spectrum analyzer (OSA) is used as a spectrum detecting device on which the spectral response can be observed.

To improve the sensing properties, the dual symmetrical PCF device is designed and analyzed as shown in Fig. 10. The fundamental mode of dual symmetrical PCF can be divided into four types according to the polarization direction: y even mode in the same direction, y odd mode in the opposite direction, x even mode in the same direction, and x odd mode in the opposite direction. The electric field distributions of core modes are as shown in Fig. 11. Generally speaking, the resonance caused by the even mode is stronger, so the loss curve of the even mode in the y direction is chosen as the research mode of the dual symmetrical PCF.

Figure 12 shows the confinement loss spectra of the sensor with the dual symmetrical PCF for the temperature range between 20 and 320 °C. The average spectral sensitivity of 3.166 nm/°C and maximum spectral sensitivity of 5.000 nm/°C can be accomplished and the corresponding temperature resolution is 0.0200 °C. The results reveal that the dual symmetrical PCF structure delivers better sensing performance than the single PCF structure for the same structural parameters.

The fitted polynomial curves of the resonant wavelength and temperature are plotted in Fig. 13. The empirical

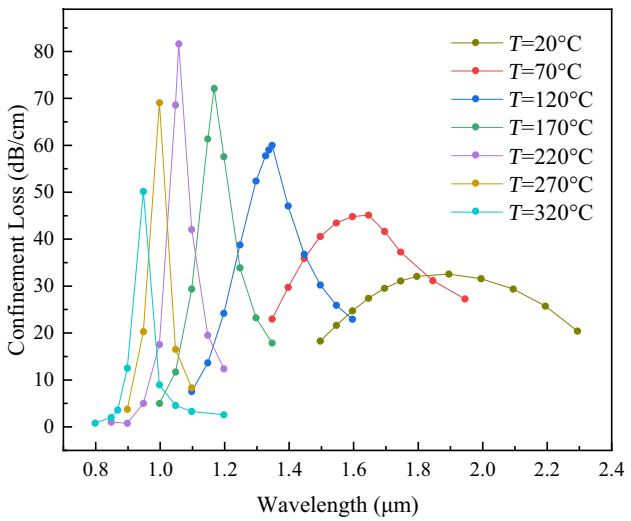

Fig. 12 Confinement loss spectra of the sensor with the symmetrical PCF structure for the temperature range between 20 and 320 °C

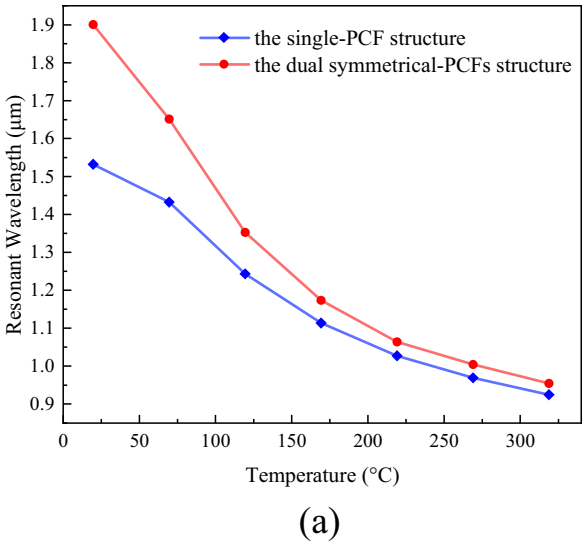

(a)

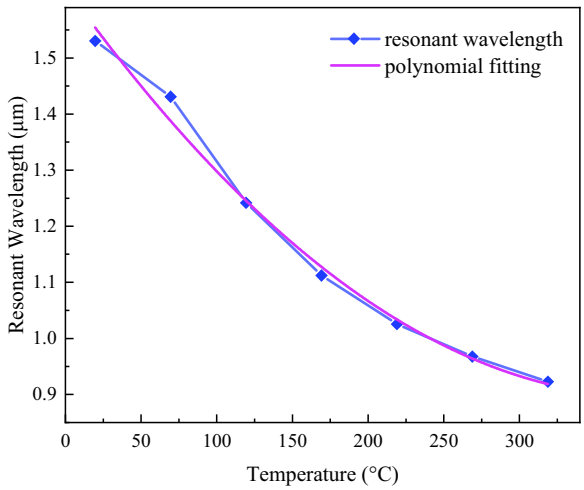

(b)

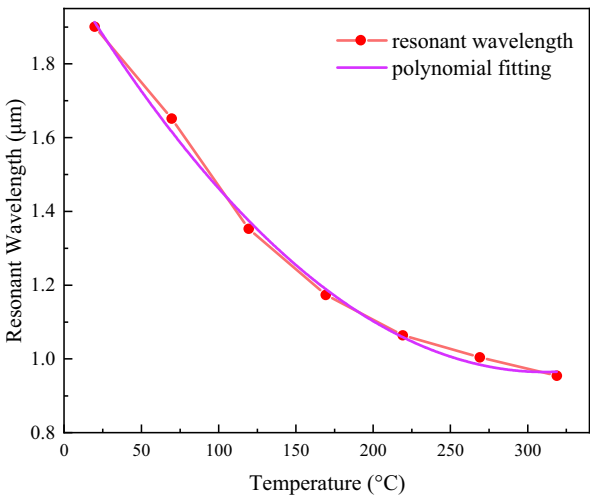

(c)

Table 1 Comparison of some published sensors for temperature sensing

Ref.	Temperature	Wavelength	Temperature sensitive liquid
[19]	35–100 °C	550–900 nm	PDMS
[29]	0–60 °C	600–1000 nm	Chloroform
[30]	− 70–70 °C	500–750 nm	Ethanol
[38]	− 50–100 °C	600–1600 nm	Mixture of toluene and chloroform
[39]	0–80 °C	450–1250 nm	Toluene
[40]	0–100 °C	550–640 nm	MF-material
[41]	20–80 °C	500–1000 nm	Glycerin
[42]	20–40 °C	1100–1700 nm	Diethylene glycol
[43]	0–80 °C	500–900 nm	Ethanol
[44]	36–86 °C	550–1375 nm	Toluene
In this paper	20–360 °C	800–2300 nm	[BMim][PF6]

equations for the single PCF structure and dual symmetrical PCFs structure are:

$$y = 1.62738 - 0.003788x + 4.86e^{-6}x^2 \quad \text{(single mode)} \quad (7)$$

$$y = 2.04589 - 0.00696x + 1.114e^{-5}x^2 \quad \text{(dual} - \text{PCFs)} \quad (8)$$

The blue and red curves in Fig. 13(a) represent the single PCF structure and dual symmetrical PCF structure, respectively. The adjusted R^2 values of these two structures are 0.98737 and 0.99475 and the COD values are 0.99185 and 0.9965, respectively. Therefore, the dual symmetrical PCF structure shows a better fitted curve. Table 1 summarizes the sensing properties of some published sensors for simultaneous measurement of temperature. As shown in Table 1, compared with many reported PCF-SPR sensors, the proposed sensor has a larger detection range.

Conclusion

A PCF-SPR temperature sensor consisting of dual embedded silver wires is designed and investigated by the FEM method as well as effective refractive index method based on the COMSOL Multiphysics software. The simulation results show that a blue-shift occurs with increasing temperature due to the filling ionic liquid [BMim] [PF_6] and the characteristics of the structure with dual symmetrical PCFs are better than those of the single PCF. To optimize the sensing performance in the temperature between 20 and 320 °C, the structural parameters such as the radius of the air holes, depth of corroded channels, and metallic materials are evaluated critically. The single PCF structure shows an average spectral sensitivity of 2.033 nm/°C, maximum sensitivity of 3.900 nm/°C, as well as temperature resolution of 0.0256 °C. In comparison, the structure based on dual symmetrical PCFs delivers better performance as manifested by an average spectral sensitivity of 3.166 nm/°C, maximum sensitivity of 5.000 nm/°C, and temperature resolution of 0.0200 °C.

Acknowledgements This work was jointly supported by the Guiding innovation Foundation of Northeast Petroleum University [Grant Numbers 2018YDL-02], Local Universities Reformation and Development Personnel Training Supporting Project from Central Authorities [Grant Number 140119001],Natural Science Foundation of Heilongjiang Province [Grant Number E2017010], and City University of Hong Kong Strategic Research Grant (SRG) [Grant Numbers 7005105 and 7005265].

Declarations

Conflict of interest The authors declare no conflicts of interest.

References

1. H.Y. Fu, S.W. Zhang, H. Chen, J. Weng, Graphene enhances the sensitivity of fiber-optic surface plasmon resonance biosensor. IEEE Sens. J. **15**(10), 5478–5482 (2015)
2. W.L. Ng, A.A. Rifat, W.R. Wong, G.A. Mahdiraji, F.M. Adikan, A novel diamond ring fiber-based surface plasmon resonance sensor. Plasmonics **13**(4), 1165–1170 (2018)
3. J.B. Lou, T.L. Cheng, S.G. Li, High sensitivity photonic crystal fiber sensor based on dual-core coupling with circular lattice. Opt. Fiber Technol. **48**, 110–116 (2019)
4. C. Li, B. Yan, J. Liu, Refractive index sensing characteristics in a D-shaped photonic quasi-crystal fber sensor based on surface plasmon resonance. J. Opt. Soc. Am. A **36**(10), 1663–1668 (2019)
5. Y. Li, Y. Liu, Z. Liu, Q. Tang, L. Shi, Q. Chen, G. Du, B. Wu, G. Liu, L. Li, Grating assisted ultra-narrow multispectral plasmonic resonances for sensing application. Apex **12**, 072002 (2019)
6. L.X. Li, Y.Z. Liang, J.Y. Guang, W.L. Cui, X.P. Zhang, J.F. Masso, W. Peng, Dual Kretschmann and Otto configuration fiber surface plasmon resonance biosensor. Opt. Express **25**(22), 26950–26957 (2017)
7. W.W. Lam, L.H. Chu, C.L. Wong, Y.T. Zhang, A surface plasmon resonance system for the measurement of glucose in aqueous solution. Sens. Actuat. B Chem **105**, 138–143 (2005)
8. Y. Chen, Z. Huang, F. Yu et al., Photoionization-assisted, high-efficiency emission of a dispersive wave in gas-filled hollow-core photonic crystal fibers[J]. Opt. Express **28**(11), 17076–17085 (2020)

9. J.L. Han, E.X. Liu, J.J. Liu, Circular gradient-diameter photonic crystal fiber with large mode area and low bending loss. J. Opt. Soc. Am. A **36**, 533–539 (2019)
10. M. Eid, M. Habib, M. Anower et al., Hollow core photonic crystal fiber (PCF)–Based optical sensor for blood component detection in terahertz spectrum[J]. Braz. J. Phys. **51**(4), 1017–1025 (2021)
11. J. Tian, C. Xu, S. Cui et al., A photonic crystal fiber-based biosensor with quasi-D-shaped layout and ITO-graphene combination[J]. Plasmonics **16**(5), 1451–1460 (2021)
12. N. Ayyanar, K.V. Sreekanth, G.T. Raja et al., Photonic crystal fiber-based reconfigurable biosensor using phase change material[J]. IEEE Trans. Nanobiosci. **20**(3), 338–344 (2021)
13. X. Wang, J. Zhu, Y. Xu et al., A novel plasmonic refractive index sensor based on gold/silicon complementary grating structure[J]. Chin. Phys. B **30**(2), 024207 (2021)
14. Z. Yan, X. Lu, W. Du et al., Ultraviolet graphene ultranarrow absorption engineered by lattice plasmon resonance[J]. Nanotechnology **32**(46), 465202 (2021)
15. J. Chen, H. Nie, C. Tang et al., Highly sensitive refractive-index sensor based on strong magnetic resonance in metamaterials[J]. Appl. Phys. Express **12**(5), 052015 (2019)
16. H.W. Lee, M.A. Schmidt, H.K. Tyagi, L.P. Sempere, P.S. Fussell, Polarization-dependent coupling to plasmon modes on submicron gold wire in photonic crystal fiber. Appl Phys Lett **93**, 111102 (2008)
17. B. Han, Y.N. Zhang, E. Siyu et al., Simultaneous measurement of temperature and strain based on dual SPR effect in PCF. Opt. Laser Technol. **113**, 46–51 (2019)
18. H. Liu, H. Wang, C. Chen et al., Highly sensitive and temperature-compensated fiber bending sensing based on directional resonance coupling in photonic crystal fibers. Opt. Fiber Technol. **47**(25), 164–171 (2019)
19. Y. Wang, Q. Huang, W. Zhu et al., Novel optical fiber SPR temperature sensor based on MMF-PCF-MMF structure and gold-PDMS film: erratum[J]. Opt. Express **27**(8), 10813–10813 (2019)
20. J.J. Butler, A.S. Bowcock, S.R. Sueoka et al., Optical properties of solid-core photonic crystal fibers filled with nonlinear absorbers[J]. Opt. Express **21**(18), 20707–20712 (2013)
21. H. Li, M.X. Low, R.T. Ako et al., Terahertz waveguides: broadband single-mode hybrid photonic crystal waveguides for terahertz integration on a chip. Adv. Mater. Technol. **5**, 2000117 (2020)
22. R. Ding, S. Hou, D. Wang et al. Novel design of a diamond-core photonic crystal fiber for terahertz wave transmission[C], 2017 Progress In Electromagnetics Research Symposium-Spring (PIERS). IEEE, 1148–1151 (2017)
23. M.S.A. Gandhi, S. Sivabalan, P.R. Babu et al., Designing a biosensor using a photonic quasi-crystal fiber[J]. IEEE Sens. J. **16**(8), 2425–2430 (2016)
24. F. Wang, L. Hu, W. Xu et al., Manipulating refractive index, homogeneity and spectroscopy of Yb3+-doped silica-core glass towards high-power large mode area photonic crystal fiber lasers. Opt. Express **25**(21), 25960 (2017)
25. S. Sridevi, J. Mohanraj, M. Valliammai, Refractive Index based Biosensor using Photonic Quasi Crystal Fiber for Detection of Metastasis Tumor cells in brain[C]//2019 Workshop on Recent Advances in Photonics (WRAP). IEEE, 1–3 (2019)
26. E. Liu, S. Liang, J. Liu, Double-cladding structure dependence of guiding characteristics in six-fold symmetric photonic quasi-crystal fiber[J]. Superlattices Microstruct. **130**, 61–67 (2019)
27. Y. Zhao, Z.Q. Deng, H.F. Hu, Fiber-optic SPR sensor for temperature measurement. IEEE Trans. Instrum. Meas. **64**(11), 3099–3104 (2015)
28. N. Luan, R. Wang, W. Lv, Y. Lu, J. Yao, Surface plasmon resonance temperature sensor based on photonic crystal fibers randomly filled with silver nanowires. Sens. (Basel) **14**(9), 16035–16045 (2014)
29. A.B. Siddik, S. Hossain, A.K. Paul et al., High sensitivity property of dual-core photonic crystal fiber temperature sensor based on surface plasmon resonance[J]. Sens. Bio-Sens. Res. **29**, 100350 (2020)
30. M.R. Islam, M.M.I. Khan, F. Mehjabin et al., Design of a fabrication friendly & highly sensitive surface plasmon resonance-based photonic crystal fiber biosensor[J]. Results Phys. **19**, 103501 (2020)
31. X. Yang, Y. Lu, B. Liu, J. Yao, Design of a Tunable Single-PolarizationPhotonic Crystal Fiber Filter With Silver-Coated and Liquid-Filled Air Holes, IEEE Photonics Society, 1943–0655 (2017)
32. T.S. Krishna, K. Narendra, M. Gowrisankar et al., Physicochemical and spectroscopic studies of molecular interactions of 1-butyl-3-methylimidazolium hexafluorophosphate+ 2-methoxyethanol or 2-ethoxyethanol binary mixtures at temperatures from 298.15 to 323.15 K[J]. J. Molec. Liquids **227**, 333–350 (2017)
33. D.S.H. Wong, J.P. Chen, J.M. Chang et al., Phase equilibria of water and ionic liquids [emim][PF6] and [bmim][PF6][J]. Fluid Phase Equilib. **194**, 1089–1095 (2002)
34. V. Najdanovic-Visak, J.M.S.S. Esperança, L.P.N. Rebelo et al., Phase behaviour of room temperature ionic liquid solutions: an unusually large co-solvent effect in (water+ ethanol)[J]. Phys. Chem. Chem. Phys. **4**(10), 1701–1703 (2002)
35. B. Gauvreau, A. Hassani, M.F. Fehri, A. Kabashin, M. Skorobogatiy, Photonic bandgap fiber-based surface plasmon resonance sensors. Opt. Express **15**(18), 11413–11426 (2007)
36. C. Du, Q. Wang, H. Hu, Y. Zhao, Highly sensitive refractive index sensor based on four-hole grapefruit microstruc- tured fiber with surface plasmon resonance. Plasmonics **12**(6), 1961–1965 (2017)
37. Y. Yu, X. Li, X. Hong, Y. Deng, K. Song, Y. Geng, H. Wei, W. Tong, Some features of the photonic crystal fiber temperature sensor with liquid ethanol filling. Opt. Express **18**(15), 15383–15388 (2010)
38. F. Wang, Z. Sun, T. Sun et al., Highly sensitive PCF-SPR biosensor for hyperthermia temperature monitoring[J]. J. Opt. **47**(3), 288–294 (2018)
39. H. Liu, H. Li, Q. Wang et al., Temperature-compensated magnetic field sensor based on surface plasmon resonance and directional resonance coupling in a D-shaped photonic crystal fiber[J]. Optik **158**, 1402–1409 (2018)
40. H. Liu, Y. Wang, C. Tan et al., Simultaneous measurement of temperature and magnetic field based on cascaded photonic crystal fibers with surface plasmon resonance[J]. Optik **134**, 257–263 (2017)
41. P.B. Bing, Z.Y. Li, J.Q. Yao et al., A photonic crystal fiber based on surface plasmon resonance temperature sensor with liquid core[J]. Mod. Phys. Lett. B **26**(13), 311 (2012)
42. B.H. An, Y.N. Zhang, X. Wang et al., High-sensitive fiber anemometer based on surface plasmon resonance effect in photonic crystal fiber[J]. IEEE Sens. J. **9**, 1–1 (2019)
43. A. Chen, Z. Yu, B. Dai et al., Highly sensitive detection of refractive index and temperature based on liquid-filled D-shape PCF[J]. IEEE Photonics Technol. Lett. **33**(11), 529–532 (2021)
44. H. Liang, T. Shen, Y. Feng et al., A surface plasmon resonance temperature sensing unit based on a graphene oxide composite photonic crystal fiber[J]. IEEE Photonics J. **12**(3), 1–11 (2020)